



Article

Post-Earthquake Traffic Simulation Considering Road Traversability

Yingying Wu ¹, Zhen Xu ^{1,*} Chenxi Liang ¹ and Ruizhuo Song ²

¹ Beijing Key Laboratory of Urban Underground Space Engineering, School of Civil and Resource Engineering, University of Science and Technology Beijing, Beijing 100083, China

² School of Automation and Electrical Engineering, University of Science and Technology Beijing, Beijing 100083, China

* Correspondence: xuzhen@ustb.edu.cn; Tel.: +86-10-6233-3268

Abstract: Post-earthquake road traversability is a critical factor that affects traffic conditions. Therefore, a post-earthquake traffic simulation method considering road traversability was proposed in this study. First, the impact ranges of the earthquake-induced building collapse and the post-earthquake fire spread of buildings were analyzed, and road traversability was determined accordingly. Subsequently, the post-earthquake traffic flow was predicted based on building characteristics, and micro-level vehicle behaviors were simulated considering post-earthquake road traversability to determine the traffic conditions. In addition, the simulation model was validated using actual data. Finally, a segment of the Tongzhou road network in Beijing was selected as a case study to analyze post-earthquake road traversability and simulate traffic conditions on critical road sections. The proposed method can provide post-earthquake traffic conditions, which benefits the decision-making of post-earthquake evacuation and rescue.



Citation: Wu, Y.; Xu, Z.; Liang, C.; Song, R. Post-Earthquake Traffic Simulation Considering Road Traversability. *Sustainability* **2022**, *14*, 11145. <https://doi.org/10.3390/su141811145>

Academic Editors: Chong Xu, Su Chen and Shuang Li

Received: 31 July 2022

Accepted: 1 September 2022

Published: 6 September 2022

Publisher's Note: MDPI stays neutral with regard to jurisdictional claims in published maps and institutional affiliations.



Copyright: © 2022 by the authors. Licensee MDPI, Basel, Switzerland. This article is an open access article distributed under the terms and conditions of the Creative Commons Attribution (CC BY) license (<https://creativecommons.org/licenses/by/4.0/>).

1. Introduction

Post-earthquake traffic conditions are directly affected by road traversability. Currently, modern roads in urban areas are built using important seismic measures with sufficient roadbeds and advanced facilities [1]. However, the debris generated by building collapses during an earthquake can fall on the surrounding road network, affecting traffic conditions [1,2]. Furthermore, rapidly spreading post-earthquake fires can endanger passing vehicles. Therefore, after an earthquake, urban roads can be blocked by collapsed buildings or post-earthquake fires, placing heavy pressure on post-earthquake rescue and recovery work [3]. For example, roads were severely blocked by collapsed buildings in the 1999 Kobe earthquake, hampering rescue activities [4]. Clearly, simulating traffic conditions is essential for efficient post-earthquake rescue and evacuation efforts. Furthermore, it is necessary to consider post-earthquake road traversability when simulating urban road traffic conditions.

The impact range of building debris has been examined by several studies [1,2,5–7]. For instance, Argyroudis et al. [8] proposed a systemic seismic risk assessment method for road networks which can be used to determine the possibility of blocked roads owing to the collapse of adjacent buildings during an earthquake. Lo et al. [9] analyzed road congestion caused by road liquefaction and building collapse according to the peak ground acceleration (PGA). Though Hirokawa and Osaragi [10] considered both collapse debris and spreading fires in a simulation of urban earthquake damage, they did not consider the impact of fires on road blockage. These studies analyzed post-earthquake road traversability considering building collapse impact but lacked the impact of post-earthquake fires.

Post-earthquake traffic can be described using either macro-level or micro-level simulations. Macro-level simulations focus on the flow of vehicles to accurately predict the distribution of traffic flow on urban roads, whereas micro-level simulations focus on the movement track of a single vehicle to reflect traffic conditions. Generally, existing post-earthquake traffic simulations have typically been conducted on the macro level [11,12], ignoring micro-level behaviors, such as vehicle-following and lane-changing. For example, Chang et al. [13] simulated post-earthquake traffic conditions considering bridge damage and post-earthquake travel behaviors under extreme conditions, focusing on macro-level performance indexes, such as the traffic capacity. Feng et al. [14] considered vehicle-following behavior and used an agent-based model to simulate post-earthquake traffic but ignored the traffic congestion caused by vehicle lane-changing behavior.

In summary, the simulation of post-earthquake traffic considering road traversability still faces two major challenges:

- (1) How can road traversability be evaluated under the impacts of multiple disasters?

After an earthquake, roads are likely to be covered by debris from collapsed buildings, limiting road traversability or even blocking roads. Furthermore, the spread of post-earthquake fires can also obstruct road access. It is difficult to systematically evaluate post-earthquake road traversability owing to the coupling relationship between the impact ranges and effects of these different disasters, as well as the time-varying spread of secondary fires.

- (2) How can the traffic conditions considering post-earthquake blocked roads be simulated on the micro level?

In the event of an earthquake, some roads will be blocked, often leading to specific micro-level behaviors, such as vehicle-following and lane-changing, that can seriously affect the traffic conditions. Thus, simulating micro-level vehicle behavior under the influence of road traversability is critical for accurate post-earthquake traffic predictions.

Many theoretical methods for earthquake damage simulation have been proposed to address the first challenge. Lu and Guan [15] proposed a multi-degree-of-freedom (MDOF) model for high-precision urban earthquake damage simulation, which can predict the earthquake damage of every floor of every building in a given area [16]. Nishino et al. [17] proposed a road blockage probability model based on an assumed trigonometric distribution to predict the scope of debris created by building collapse. However, no method published to date has clearly defined the impact of post-earthquake fires on road traversability. Therefore, the impact of post-earthquake fires on road traversability needs to be considered in this study.

Developing traffic simulation technologies offer various approaches for the micro-level analysis of road traffic conditions to address the second challenge [13,18]. Song and Sun [19] calibrated the parameters affecting the micro-level vehicle behavior using sensitivity analysis to control the vehicle-following and lane-changing behaviors. Furthermore, existing traffic simulation systems provide a visual window for micro-level traffic simulation to intuitively express vehicle behavior [20]. However, the influence of road traversability on micro-level vehicle behavior should be directly considered to accurately simulate post-earthquake traffic conditions.

To address these challenges, a post-earthquake traffic simulation method that considers road traversability was proposed in this study. First, the collapse and post-earthquake fire spread in a building complex were analyzed to determine the impact range under multiple disasters, and then, the road traversability was analyzed. Next, the post-earthquake traffic flow was predicted based on building characteristics, and micro-level vehicle behaviors were simulated considering post-earthquake road traversability to determine the traffic conditions. In addition, the simulation model was validated using actual data. Finally, a segment of the Tongzhou road network in Beijing was taken as a case study to predict the post-earthquake road traversability and simulate the traffic conditions of critical road

sections. Thus, the proposed method can provide post-earthquake traffic conditions which benefits the decision-making of post-earthquake evacuation and rescue.

2. Framework

The research framework employed in this study is shown in Figure 1, which is made of three components as follows:

1. Road Traversability Analysis

First, the seismic response of the building group was calculated using the MDOF model, and then, the corresponding impact range of collapse debris was analyzed. Then, the process of fire spreading between buildings was analyzed to determine its impact range. Finally, the impact ranges of collapse debris and post-earthquake fires were overlapped to analyze road traversability.

2. Post-Earthquake Traffic Simulation

First, resident travel behaviors were predicted based on building characteristics to determine traffic flow distribution on the roads. Then, the traffic model on the VISSIM platform was modified using the local parameters, and micro-level vehicle behaviors on critical road sections were simulated considering the post-earthquake road traversability and traffic flow distribution. Finally, the modified traffic model was validated by comparing the actual measured traffic data of the sections.

3. Case Study

A segment of the Tongzhou road network in Beijing was used as a case study, and the post-earthquake traffic conditions of this segment were simulated considering road traversability.

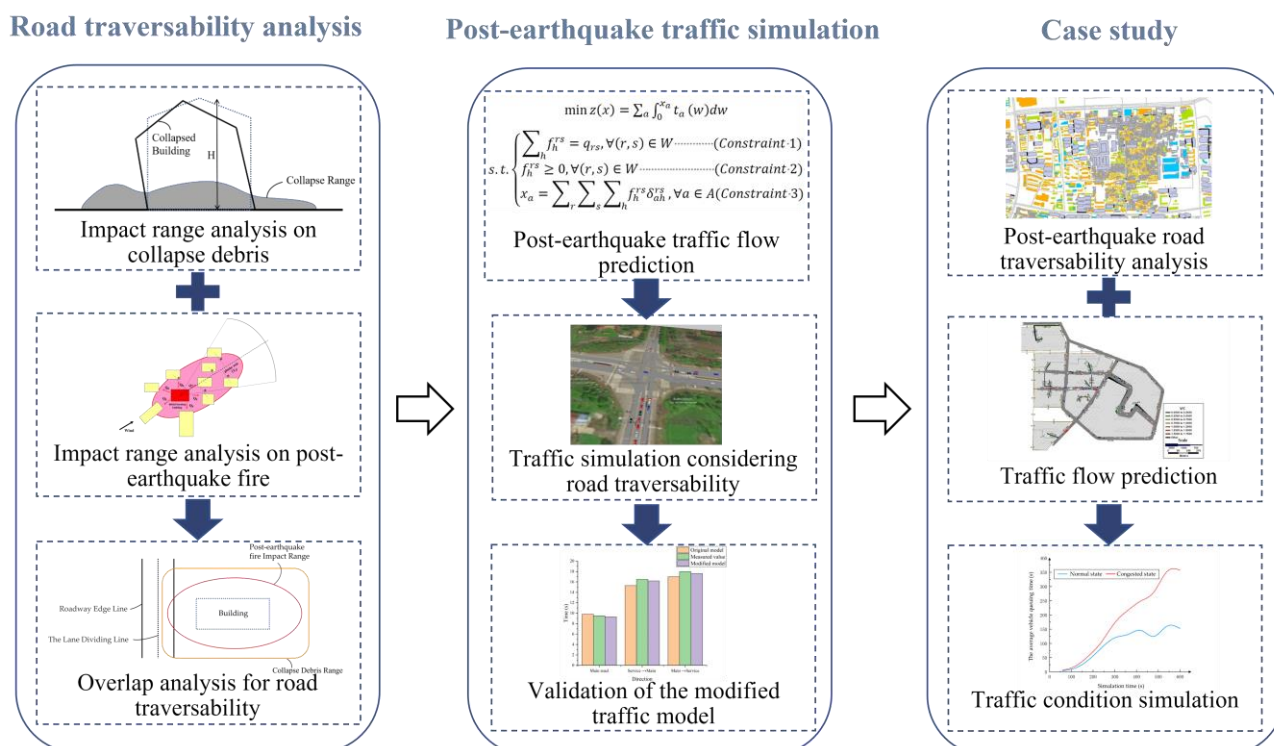


Figure 1. Research framework.

3. Method

3.1. Road Traversability Analysis Considering the Impact of Multiple Disasters

The effects of multiple disasters—an earthquake followed by fires—on the road network were considered in the road traversability analysis.

Understanding the seismic response of the buildings is an essential prerequisite for analyzing the impact range of the earthquake-induced building collapse and the post-earthquake fire spread of buildings. However, it is difficult to establish a refined structural model for each building in a densely constructed urban area. Therefore, in this study, the MDOF model proposed by Lu and Xiong [21,22] was used to rapidly compute the seismic response parameters of buildings, including the damage severity, floor displacement, and acceleration. On this basis, the impact ranges of collapse debris and post-earthquake fires were studied. It should be noted that earthquake-induced damage to urban roadways was not considered in this study since the quality of the roadbed in urban areas is normally sufficient to prevent major damage from an earthquake, and damage to the road surface has little impact on vehicle free passage.

3.1.1. Impact Range Analysis on Collapse Debris

Through the investigation of the earthquake damage caused by the Great Hanshin Earthquake, Nishino et al. [17] have obtained the probability equation of the building's collapse scope. Therefore, the collapse debris distribution probability model proposed by Nishino et al. was employed in this study to calculate the effective impact range of collapse debris given by Equation (1):

$$\frac{H}{8} < w_0 < \frac{H}{2} \quad (1)$$

where H is the height of the building with the collapse range (w_0) of the building between $H/8$ and $H/2$. To highlight the impact caused by collapse debris, the maximum impact range ($H/2$) was used to conduct a relative analysis in this study. The unit of H here is meters (m), as the same below.

Thus, the collapse debris impact range, w , owing to an earthquake can be calculated as shown in Equation (2):

$$w = \frac{H}{2} \quad (2)$$

Additionally, the safety cordon of buildings that are likely to collapse (i.e., buildings with extensive or moderate damage) can also be determined by Equation (2) because the maximum impact range of building collapse (i.e., w) is employed for the cordons according to Equation (1). Through the safety cordon, people are warned to stay a safe distance (i.e., w) from the dangerous building, which can prevent accidents and further casualties in the post-earthquake environment.

3.1.2. Impact Range Analysis on Post-Earthquake Fire

Post-earthquake fire is a common secondary hazard induced by earthquakes [23,24]. Historically, some severe post-earthquake fire events have occurred in major cities worldwide, such as those in San Francisco in 1906 [25], Tokyo in 1923 [26], and Osaka and Kobe in 1995 [27]. The post-earthquake fires spread rapidly, which may seriously affect vehicle passage on the surrounding roads. Therefore, the process of fire spreading between buildings was analyzed in this study to determine their impact range.

First, the locations of fire initiation were identified. The fire quantity, N , under a given PGA was obtained using the method proposed by Ren and Xie [28] according to a regression of historical post-earthquake fire data (e.g., San Francisco Earthquake in 1906 and Tokyo Earthquake in 1923). The first N buildings with the highest fire probabilities were then chosen as the fire initiation points after calculating the fire probability of buildings with various damage severities.

The regional fire quantity, N , under the selected PGA can be calculated according to Equation (3):

$$N = -0.11749 + 1.34534PGA - 0.8476PGA^2 \quad (3)$$

where N is the number of buildings on fire per 100,000 square meters, and the unit of PGA is g.

After normalization, the fire probability of buildings according to damage severity can be represented by the fire index, r_0 , calculated as shown in Equation (4):

$$r_0 = \frac{P(M) \times P(F_k|M) \times \sum_j [P(D_j|PGA) \times P(C_j|D_j) \times P(S_j|D_j)] \times P(G)}{0.867} \quad (4)$$

The fire probability of each building will be calculated and sorted according to Equation (4), and the first N buildings with the highest fire probability will be designated as the fire points. For detailed meanings of all parameters given above, as well as their values, please refer to Table 1.

Table 1. Parameter related to the building fire index.

Parameter	Meaning	Value
$P(M)$	Probability that the structure contains combustibles.	Set the value to 1 if the structure contains combustibles; set it to 0 if it does not.
$P(F_k/M)$	Probability that a building fire is affected by a specific combustible.	Set the value according to the flammability of the building's interior materials and the building itself.
$P(G)$	Probability that a building fire is affected by weather and other factors.	Set different values based on variables, such as weather.
$P(C_j/D_j)$	Probability that inflammable material leakage in buildings under the damage state, D_j .	Set the value according to the damage severities.
$P(S_j/D_j)$	Probability that a fire will break out inside a building in the damage severities, D_j .	Set the value according to the damage severities.
$P(D_j/PGA)$	Probability that a building will fail in state D_j under a specific PGA.	Set the value according to the outcomes of regional seismic response simulations for buildings.

Second, the process of post-earthquake fires spreading between buildings was analyzed. The post-earthquake fires spreading model for buildings proposed by Lu et al. [23] was used to perform a relative analysis. This model considers two factors when analyzing the spread of fire: the thermal radiation and the thermal plume (as shown in Figure 2). A burning building affects the adjacent buildings via the thermal radiation of the flame through the doors, windows, and external walls and affects the buildings in the downwind direction via the thermal plume of high-temperature flue gas. If the heat flux received by an unburned building within a certain period of time exceeds its critical value under the common influence of the surrounding burning buildings, it can be assumed that the building is about to combust.

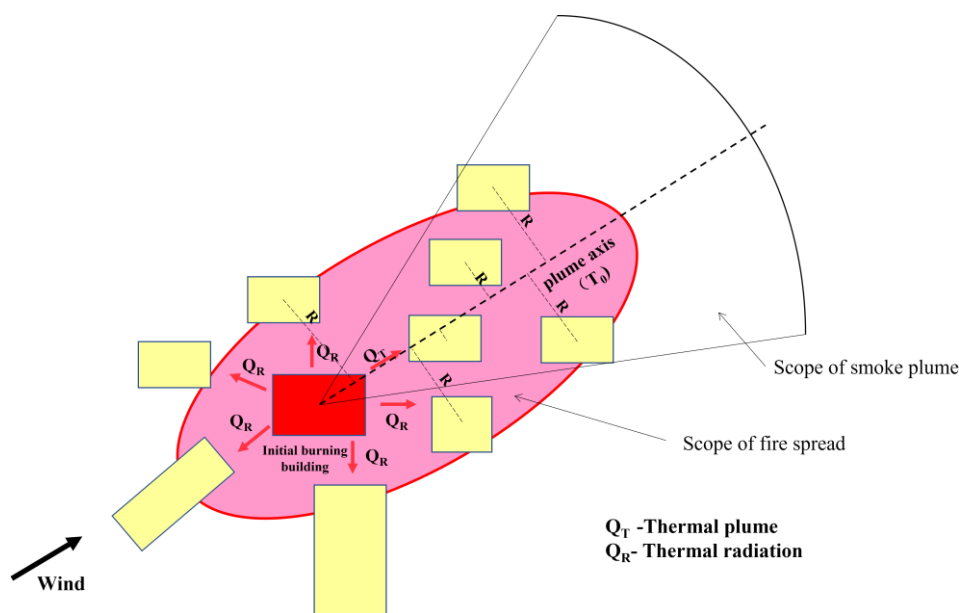


Figure 2. The process of post-earthquake fires spreading.

Buildings may be more prone than usual to fire following an earthquake because of the reduced capacity for prevention. The model used in this study was designed based on concepts presented by Himoto et al. [29] who assumed that the building damage caused by an earthquake reduces the ultimate heat flux threshold for building fire, \dot{q}_{cr} , as shown in Equation (5):

$$\dot{q}_{cr} = \phi \dot{q}_{cr,H} + (1 - \phi) \dot{q}_{cr,L} \quad (5)$$

where ϕ is the damage factor of the envelope material, and $\dot{q}_{cr,H}$ and $\dot{q}_{cr,L}$ are the limit heat flux when $\phi = 1$ and $\phi = 0$, respectively. For the values of these parameters, please refer to [29].

Finally, the impact range of post-earthquake fires was determined. When the distance between adjacent buildings reaches a certain threshold, the fire cannot spread from building to building; this distance is generally considered the limit distance of fire spread [30]. As most urban buildings meet the requirements of the design fire code, the fire separation distance between buildings is typically greater than the limit distance of fire spread. Therefore, though the maximum impact range of a post-earthquake fire is technically dependent on the limit distance of fire spread, the most adverse impacts of post-earthquake fire on road traversability in this study were evaluated using the fire separation distance representing the post-earthquake fire impact range, f , which is given by Equation (6):

$$F_{\text{limit distances}} \leq F_{\text{fire separation distance}} = f \quad (6)$$

Please refer to Table 2 for specific fire separation distances between different buildings, which comes from the code for fire protection design of buildings in China [31].

Table 2. The fire separation distance of civil building.

Building Classification	High-Rise Buildings		Other Civil Buildings		
	I, II	I, II	III	IV	
High-rise buildings	I, II	13 m	9 m	11 m	14 m
	I, II	9 m	6 m	7 m	9 m
Other civil buildings	III	11 m	7 m	8 m	10 m
	IV	14 m	9 m	10 m	12 m

I, II, III, and IV represent the fire resistance rating of the buildings. (Reference to the code for fire protection design of buildings of China [31]).

3.1.3. Overlap Analysis for Road Traversability

In this study, the impacts of multiple disasters on the road network were comprehensively analyzed by overlapping the collapse debris impact range and post-earthquake fire impact range. The accurate impact ranges of the earthquake-induced building collapses or fires are difficult to be calculated due to the uncertainty of earthquakes. This study aims to evaluate the worst-case scenario based on conservative design principles. Note that such a worst-case scenario is necessary for the urban planning and emergency preparedness of a city. Therefore, the maximum impact ranges of building collapse and fires are suitable for such a worst-case scenario in this study.

According to Equations (2) and (6), the collapse debris impact range and the post-earthquake fire spread impact range were calculated. Since collapse debris and post-earthquake fires both hinder road traffic, the one with a larger impact range should be considered when analyzing road traversability. Therefore, the maximum value (i.e., F_{max}) between the two impact ranges is chosen as the criterion. Then, the two results were overlapped to obtain the maximum value of the impact range F :

$$F_{max} = \max[w, f] \quad (7)$$

The greater the value of F_{max} , the more obstructed the road will be. Therefore, according to F_{max} , road traversability can be divided into the following three states using Equation (8):

$$\begin{cases} \text{Normal states,} & F_{max} < d \\ \text{Congested states,} & d \leq F_{max} < d + \frac{r}{2} \\ \text{Blocked states,} & d + \frac{r}{2} \leq F_{max} \end{cases} \quad (8)$$

where r is the width of the road and d is the distance from the building boundary to the road boundary.

In this study, the buffer area function in ArcGIS was used to analyze road traversability. First, road and building models were created in ArcGIS. Subsequently, buffer areas of the collapse debris impact range and the post-earthquake fire impact range were created. Finally, an overlap analysis was conducted on the buffer areas in ArcGIS using Equation (8) to determine the traversability of the road network.

3.2. Post-Earthquake Traffic Simulation Considering Road Traversability

3.2.1. Post-Earthquake Traffic Flow Prediction Based on Building Characteristics

The post-earthquake traffic flow, which is used to simulate post-earthquake traffic conditions, varies significantly due to changes in post-earthquake travel demand. In this study, the post-earthquake traffic flow was predicted based on the surrounding building characteristics; it comprises two parts: (1) post-earthquake origin-destination (OD) prediction and (2) allocation of traffic flow.

(1) Post-Earthquake OD Prediction

Post-earthquake OD prediction is primarily used to evaluate the total vehicle production (P) and total vehicle attraction (A) in the traffic zone after an earthquake.

Floor area per capita is a critical factor considered during building design, and to a certain extent, the area of a building is directly proportional to the population within. Therefore, according to building characteristics (etc. function and area) in each traffic zone and in accordance with relevant planning standards [32], the population data were reverse deduced in this study to achieve OD prediction.

The specific steps of this process are as follows:

Step 1: Calculate the area of the buildings with different function types in each traffic zone, S_{ij} .

Step 2: Calculate the resident population in the buildings with different function types in each zone, N_{ij} , according to Equation (9):

$$N_{ij} = \frac{S_{ij}}{A_j} \quad (9)$$

where A_j is the floor area per capita, the value of which can be referred to in Table 3.

Table 3. Floor area per capita.

Type	Floor Area Per Capita(m ²)
Residential Building	30
Industrial Building	30
Administrative Building	20
Commercial Building	20
Cultural Building	100

Step 3: Modify the travel rate (TR) and attraction rate (AR) of the various buildings after the earthquake.

Using research conducted by the China Academy of Urban Planning and Design and the Beijing Transportation Institute [33], the regular population travel rate and population attraction rate for different types of buildings were summarized and sorted as shown in Table 4.

Table 4. Reference values of trip rate and attraction rate of various buildings.

Reference Values	Building Function				
	Residential Building	Industrial Building	Administrative Building	Commercial Building	Cultural Building
Trip rate	2	2	6	7	8
Attraction rate	2	2.5	11	15	18

After an earthquake, the urban functional structure will be damaged to a certain extent. Therefore, the importance of different functional buildings in the city will change, as will travel demand and travel times; these factors should be reflected in the change in traffic flow. For example, the attraction rate of commercial sites providing consumption and entertainment will be considerably reduced, as will the traffic generated by going to work, school, and other activities. Conversely, storage land, hospitals, government offices, and residential buildings will see a significant increase in attraction rates. Therefore, the travel and attraction rates of different types of buildings should be modified, as shown in Table 5.

Table 5. Corrected values of trip rate and attraction rate of various buildings.

Corrected Values	Building Function				
	Residential Building	Industrial Building	Administrative Building	Commercial Building	Cultural Building
Trip rate	5	2.5	8	7.5	6
Attraction rate	3	1	15	8	14

Step 4: Calculate the total traffic production, E_i , and traffic attraction, F_i , in each zone as follows:

$$E_i = \sum_j N_{ij} \times TR_j \quad (10)$$

$$F_i = \sum_j N_{ij} \times AR_j \quad (11)$$

where TR_j and AR_j are the population travel rate and population attraction rate, respectively, of building type j .

Step 5: Calculate the vehicle production, P_i , and vehicle attraction, A_i , for each zone as follows:

$$P_i = E_i \times k \quad (12)$$

$$A_i = F_i \times k \quad (13)$$

where k is the proportion of vehicle travel among traffic travel modes in the region. According to the statistical data describing resident travel modes in Beijing in 2010 [34], travel by car accounted for 80% of travel; thus, $k = 0.8$. It is worth noting that the value of k should be determined based on the post-earthquake traffic travel mode. The fact that Beijing's traffic model was used in this study and there was a lack of earthquake data in Beijing means that the k mentioned in this study does not consider the changes in travel modes after the earthquake.

(2) Allocation of Traffic Flow

The primary purpose of traffic flow allocation is to study where the traffic generated by traffic zones will flow to and where the attraction comes from so that the traffic flow between traffic zones can be assigned for each road.

In this study, traffic flow was predicted based on the gravity model [35] which can be used to allocate traffic flow between zones according to the inverse relationship between the travel volume and the impedance of the zones (such as time and distance), as well as the proportional relationship between the AR and the TR. This study employed TransCAD (transportation planning software) to achieve this purpose.

The user-optimized equilibrium (UE) model [36] was used to allocate traffic flow, and its mathematical optimization model is given by Equation (14):

$$\begin{aligned} \text{min}_z(x) &= \sum_a \int_0^{x_a} t_a(w) dw \\ \text{s.t.} &\left\{ \begin{array}{ll} \sum_h f_h^{rs} = q_{rs}, \forall (r, s) \in W & (\text{Constraint 1}) \\ f_h^{rs} \geq 0, \forall (r, s) \in W & (\text{Constraint 2}) \\ x_a = \sum_r \sum_s \sum_h f_h^{rs} \delta_{ah}^{rs}, & \forall a \in A \text{ (Constraint 3)} \end{array} \right. \end{aligned} \quad (14)$$

where r_s represents the “OD pair” corresponding to any two traffic zones and h represents the total number of roads between these two zones. Constraint 1 represents the flow conservation where the sum of the travel path flow, f_h , of any r_s must be equal to the traffic flow, q , between zones. Constraint 2 mandates that the traffic value allocated to any lane between any two zones cannot be negative. Constraint 3 indicates that the road section flow in the output result is a statistical value expressed as the sum of all traffic flows passing through the road section.

The UE model is typically solved using the Frank-Wolf algorithm [37]. The core of this algorithm employs linear programming to approach a nonlinear programming problem step by step. It begins at the initial point, then takes the optimal step size as the search scope and the fastest descending direction as the forward direction to determine the starting point of the next iteration. This process is repeated to gradually approach the optimal solution and obtain the traffic flow in each section.

3.2.2. Traffic Simulation Considering Road Traversability

The traffic simulation considering road traversability after an earthquake was primarily undertaken in this study to simulate the vehicle behaviors in the presence of road obstructions and to analyze the interactions between vehicles and the traffic environment. Therefore, micro-level traffic simulation technology was employed to analyze post-earthquake vehicle behaviors considering road traversability. This simulation comprises two modules: (1) setting road conditions and (2) building the simulation model.

(1) Setting Road Conditions

The road conditions were classified into congested or blocked states according to Equation (8), which will have different impacts on road traffic. The impact of a congested

road on traffic is reflected by the inability of vehicles to use the full width of a certain length of road and thus an increase in traffic using the several lanes remaining available, as shown in Figure 3. In contrast, the impact of a blocked road on traffic is reflected by the complete inability of vehicles to pass the road section.

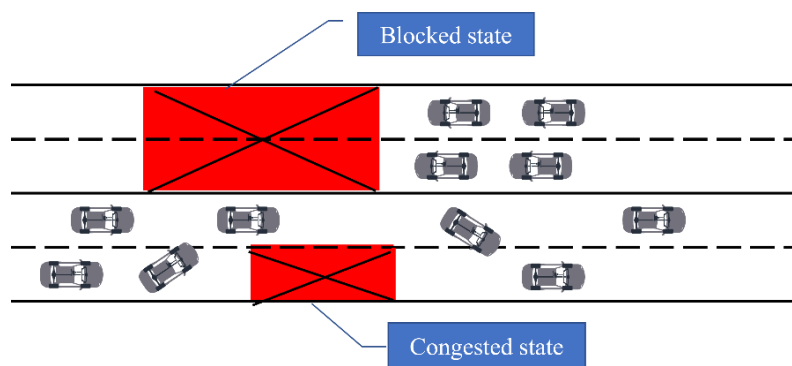


Figure 3. The setting of road conditions.

In this study, the VISSIM platform, a modeling tool used to simulate urban traffic conditions [38], was used to simulate the impact of these two states on traffic. Different measures were taken in VISSIM to simulate the different traffic states: for blocked roads, the entire road section was deleted from the simulation, whereas for congested roads, the lane shutdown option was adopted in the simulation. Additionally, the lengths of the blocked/congested road sections can be obtained from the road traversability analysis results, as described in Section 3.1.

(2) Building the Simulation Model

If a road is blocked or congested after an earthquake, vehicles may alter their original routes, resulting in different behaviors. These behaviors can be generally classified into two types: vehicle-following and lane-changing. The former represents the driving behaviors of the front and following vehicles under the ever-changing road conditions; the latter represents the vehicle behaviors changing their running lanes from one to another according to the road conditions at that time (see Figure 3). The lane-changing behaviors of vehicles critically impact the traffic-running state as they cause traffic disturbances and reduce road traversability.

A simulation model was built in VISSIM to simulate the micro-level vehicle behaviors. However, the default model parameters in VISSIM are based on traffic conditions in Germany, which differ significantly from those in China. Therefore, the simulation model parameters were adjusted according to the target national traffic situation.

There are 12 modifiable parameters in the VISSIM simulation model that describe vehicle-following and lane-changing behaviors. These parameters were modified in this study to reflect the actual situation of the case study region (Tongzhou, Beijing, China), and the results are shown in Table 6. The modified model was used to simulate the vehicle-following and lane-changing behaviors under blocked and congested road states.

3.2.3. Validation of the Modified Traffic Model

Because of the blocked or congested road after the earthquake, vehicles are likely to change lanes, resulting in traffic congestion. However, the changes before and after the earthquake are not necessary for the validation of micro-level vehicle behaviors. For instance, the daily blocked or congested roads can also cause the lane-changing behaviors. Therefore, the reliability of the modified traffic model can be validated by comparing the measured micro-level vehicle behaviors on a daily blocked or congested road with the simulation results. The entrance and exit of the main and service roads of the Guanghua Bridge located along Beijing's East 3rd Ring Middle Road were chosen to measure vehicle

behaviors in this study. By comparing the traffic simulation results and measured data in this region, the model's availability can be confirmed.

Table 6. Correction of simulated parameters.

Vehicle Behavior	Parameters	Default Values	Corrected Values
Vehicle-following	Number of visible vehicles ahead	2	4
	Average car park spacing (m)	2	2.2
	Maximum forward sight distance (m)	250	200
	Additional sections on the safe distance	2	1.08
	Multiples of the safe distance	3	3.58
Lane-changing	Waiting time before disappearing (s)	60	66.21
	Maximum deceleration (m/s^2)	-4	-5.86
	-1 m/s distance (m)	100	102.3
	Acceptable deceleration (m/s^2)	-1	-1.28
	Safe distance reduction factor	0.6	0.32
Lane-changing	Coordinated braking maximum deceleration (m/s^2)	-4	-6
	Minimum headway (m)	0.5	2

For the measured data, a field investigation was also conducted to obtain the attributes of all roads in the simulated area (Table 7). In addition, the traffic flow data describing 20 min of the morning rush hours on a certain working day were obtained from road traffic images, as shown in Table 7.

Table 7. Basic information for case sections.

Attributes of the Sections		Measured Data in Sections		
Name	Value	Direction	Number of Vehicles	Travel Time (s)
Main road	3	Go straight on the main road	1352	9.5
Service road	3	Go straight on the service road	289	\
Weaving area lanes	1 m	Service road → Main road	259	16.5
Lane width	3.25 m	Main road → Service road	181	18
Confluent section length	80 m	\	\	\

For the traffic simulation, two VISSIM models were constructed in this study: one using the modified parameters described in Table 6 (called the “modified model”) and the other using the platform default parameters (called the “original model”).

The road network was constructed in the VISSIM platform at a one-to-one ratio according to the observed road conditions with travel-time-monitoring points arranged at major sections. The monitored travel times comprised three main routes: through the main road, through the service road and then the main road, and through the main road and then the service road. After arranging the monitoring points, the default parameters were modified using the “Driving Behavior Parameter Setting” of the VISSIM platform.

Under the same input conditions, the two models were used to conduct a 600 s simulation of road traffic conditions to obtain the travel time in each road section. Figure 4 shows a visualization of the road traffic conditions obtained by the modified simulation at a given time, and the results of the two simulations are compared with the field-measured results in Table 8.

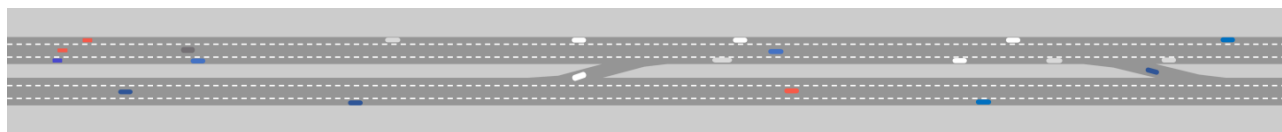


Figure 4. Simulation results at a time.

Table 8. Comparison of simulation results.

Direction	Measured Value	Original Model	Modified Model
Go straight on the main road	9.5s	9.8s	9.3s
Service road → Main road	16.5s	15.3s	16.2s
Main road → Service road	18s	17s	17.6s

It can be observed from the comparison that the revised model parameters effectively improved the accuracy of the simulation, indicating that the parameter correction scheme adopted in this study is reliable. Hence, the modified parameters were confidently applied to conduct traffic simulations in VISSIM.

4. Case Study

4.1. Case Introduction

As Beijing is located in a seismically active zone, it is likely to experience medium-strong earthquakes. In addition, the city contains dense buildings that could induce severe traffic problems in the event of an earthquake. Therefore, part of the Tongzhou district in Beijing was selected as the case study to demonstrate the simulation method. Tongzhou contains 43,881 buildings in total, as shown in the building footprint and road network model in Figure 5.

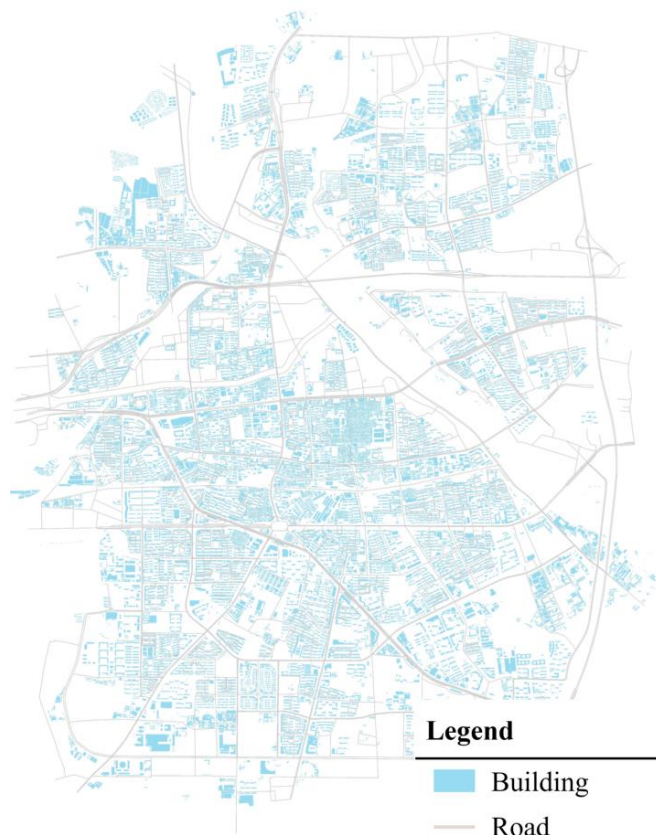


Figure 5. The building footprint and road network model.

The Sanhe–Pinggu seismic wave generated by the Institute of Geophysics, China Earthquake Administration [39] was used to construct an earthquake scenario. In this scenario, the seismic performance of buildings was analyzed by using the MDOF model [23].

4.2. Post-Earthquake Road Traversability Analysis

4.2.1. Analysis of the Debris Impact Range

The earthquake simulation results shown in Figure 6 indicate many collapsed or damaged buildings in the case study area; these will create a considerable quantity of debris that can seriously affect road traversability and hinder evacuation and post-disaster rescue. To analyze the corresponding impact on road traversability in this region, the method described in Section 3.1 was applied to calculate the debris impact range. The road traversability under the influence of building collapse is shown in Figure 6.

Figure 6 shows that collapse debris blocks many of the roads. The main roads between the residential areas are more seriously affected owing to the dense construction of buildings within, whereas the main roads of the city, being far from the surrounding buildings, are less affected.

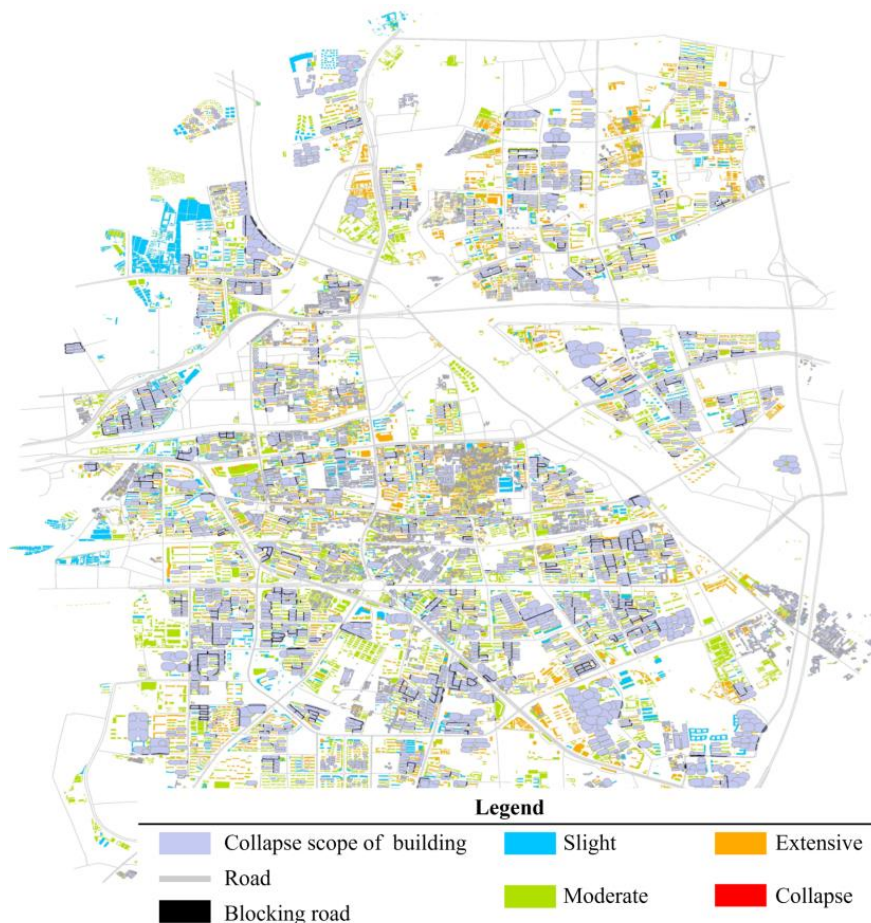


Figure 6. Road traversability under the influence of building collapse.

4.2.2. Analysis of the Post-Earthquake Fire Impact Range

The spread of post-earthquake fire between buildings will be constrained by the fire separation distance. Therefore, based on the analysis of building seismic damage, the area with the greatest fire risk was selected in this case study to analyze the post-earthquake fire spread condition within 5 h after the earthquake. For the specific results, please see Figure 7.

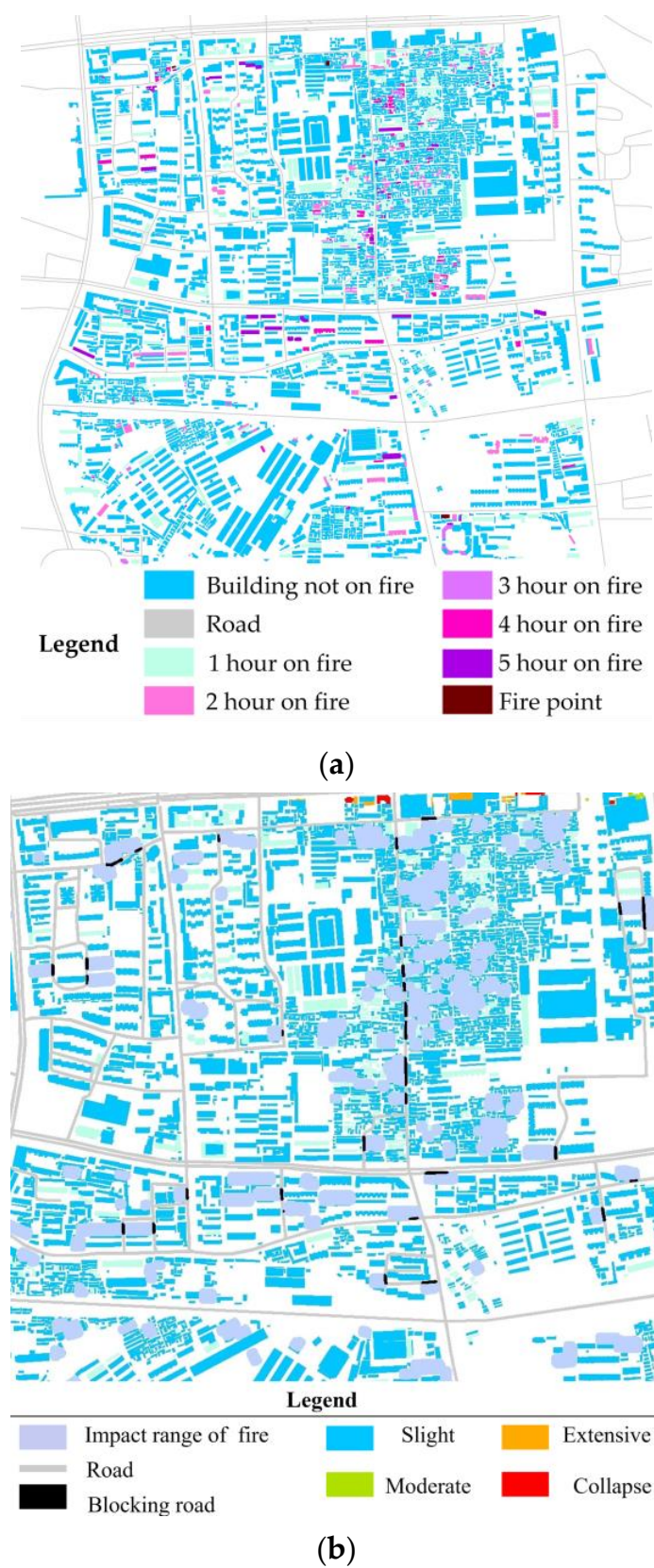


Figure 7. The spread of fire between buildings: (a) the fire time of buildings; (b) the change in road traversability.

It can be observed in Figure 7a that if a fire breaks out following an earthquake in the case study area, it will spread quickly owing to the relatively close spacing of buildings. If firefighting measures are not undertaken in time, considerable losses will be inevitable. In addition, the spread of fire has a certain impact on road traversability (Figure 7b), blocking timely rescue and evacuation efforts.

4.2.3. Comprehensive Analysis of Road Traversability

The impacts of the simulated earthquake and its post-earthquake fires were comprehensively analyzed to obtain the overall impact range under multiple disasters. Overlapping these results on the road network, all affected road sections were obtained, as shown in Figure 8.

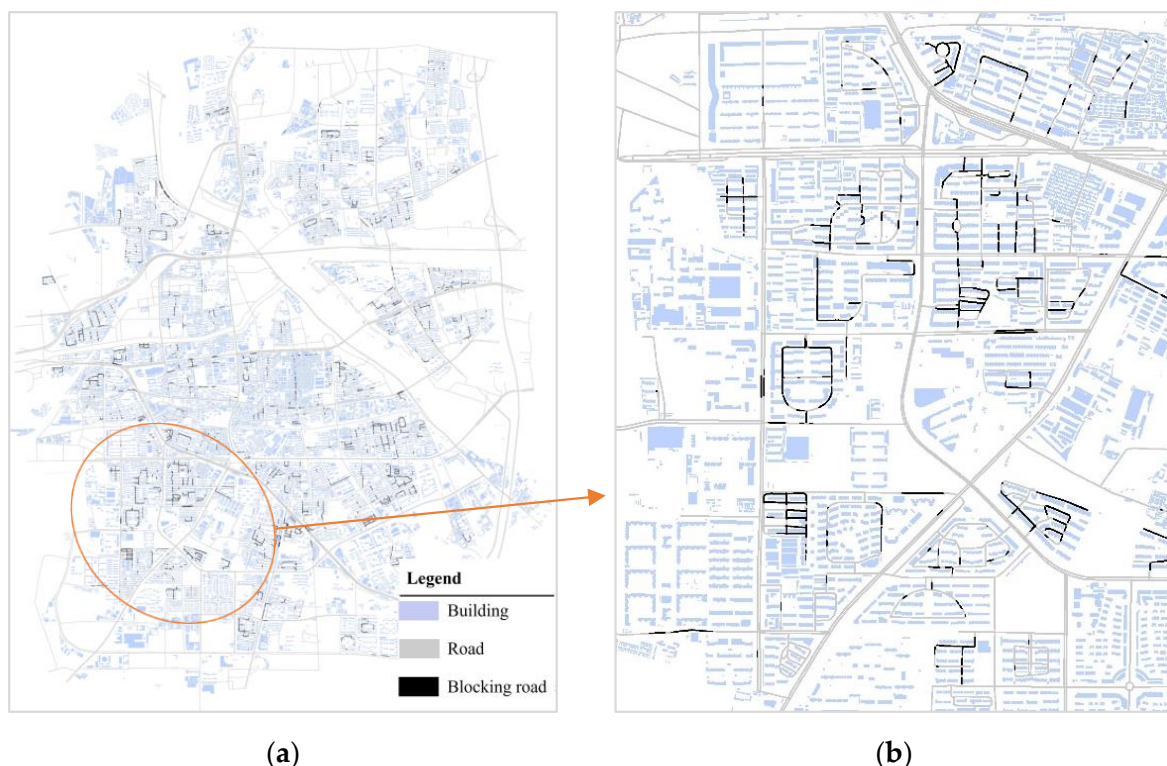


Figure 8. Comprehensive analysis of road traversability: (a) the overall situation of road traversability in the case area; (b) the local situation of road traversability in the case area.

4.3. Post-Earthquake Traffic Simulation

The traffic conditions in key road sections were studied based on the road traversability analysis results shown in Figure 8. The area in the middle of Figure 8b is located at the intersection of various traffic arteries, and the paths in each zone are severely blocked. Therefore, more attention should be paid to this region, and a traffic simulation was conducted here accordingly, as discussed in this section.

4.3.1. Post-Earthquake Traffic Flow Prediction

According to the existing road network structure, the research area was divided into eight traffic zones, as shown in Figure 9. By compiling statistics describing the floor areas corresponding to different building functions within all traffic zones, the populations were estimated and used to obtain the resident travel behaviors. The building statistics for all zones are shown in Table 9.

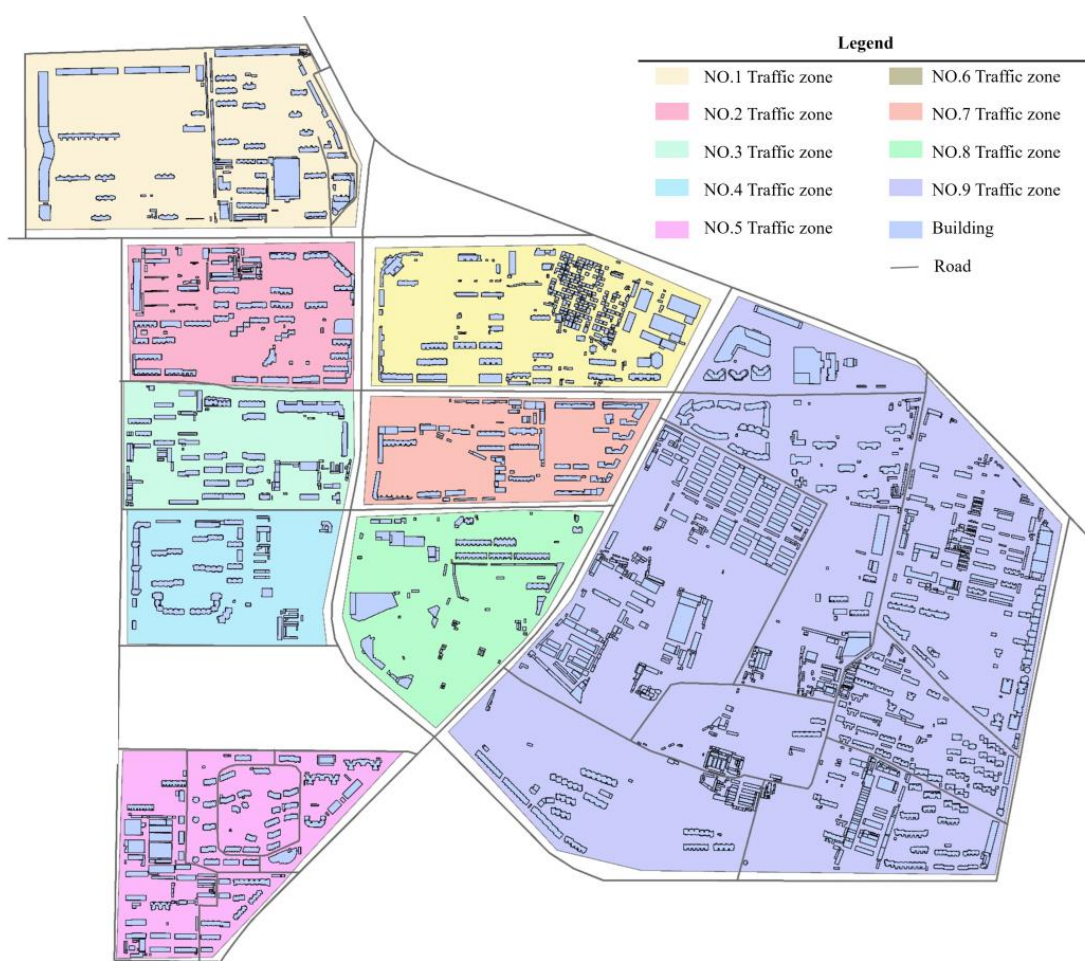


Figure 9. Division of traffic zones.

Table 9. Different types of building area statistics forms in each community (m^2).

NO.	Commercial	Industrial	Residential	Cultural	Administrative
1	26,315.36	425.78	37,053.78	2086.01	9703.69
2	26,829.91	6709.01	21,805.55	979.78	2602.53
3	15,908.85	0	19,791.15	11,826.85	759.79
4	5098.72	3891.86	7875.94	2168.29	9301.04
5	3008.17	0	39,556.54	1609.17	17,793.29
6	34,612.08	0	37,808.36	498.69	1155.78
7	18,550.2	0	14,586.98	1997.26	4459.12
8	16,330.53	0	8275.62	7872.31	2992.43
9	59,119.26	18,736.8	76,542.93	95,740.71	83,817.74

After obtaining the floor area, the post-disaster travel behaviors of the residents were predicted using the method described in Section 3.2, and the travel expectation between zones was analyzed to obtain the traffic flow. This traffic flow was then allocated to acquire the traffic flow situation on each main road, as shown in Figure 10.

The widths of the lines in the figure represent the relative scale of traffic flow, where the wider the line, the more traffic the road carries. The numbers in the figure represent the traffic flow values allocated to the roads. The colors of the lines in the figure represent the level of road service, ranging from green to red: a darker color means worse road service.

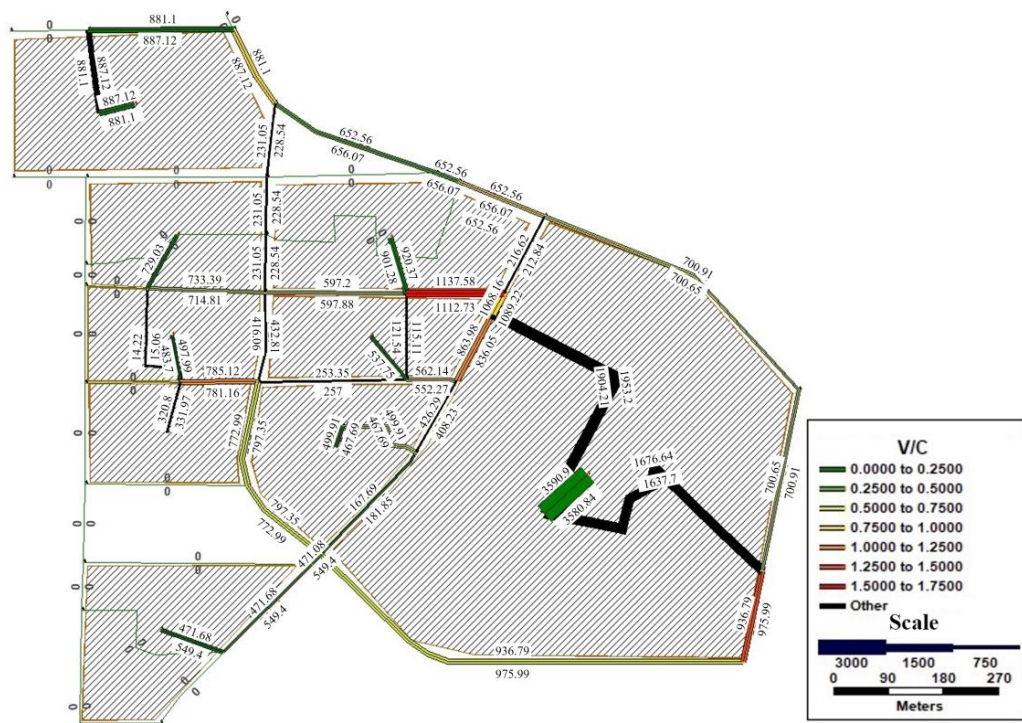


Figure 10. Allocation of traffic flow.

Using the VISSIM platform to simulate the traffic conditions for the road network model, traffic flow was set per road according to the flow results. A 600 s simulation of traffic conditions was conducted for the target area accordingly, and the traffic condition results at a certain time are shown in Figure 11.

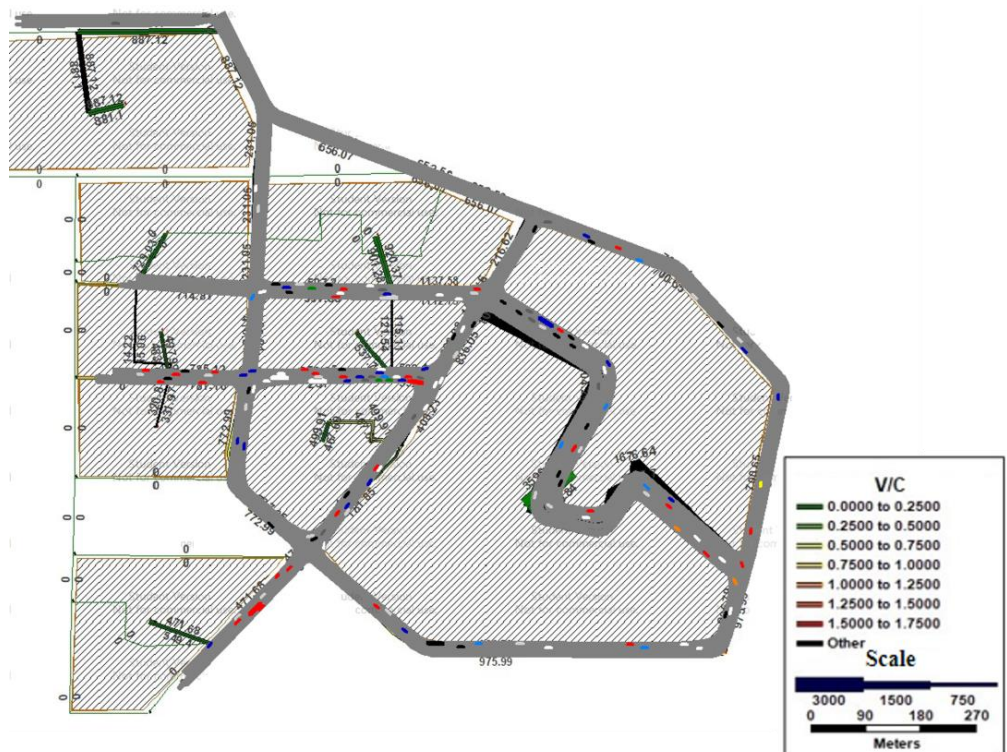


Figure 11. Traffic simulation results.

The interchange between traffic zones features heavy traffic pressure with diversified vehicles, indicating that these road sections are easily blocked following an earthquake, thus increasing the risk of vehicle congestion and traffic failure.

4.3.2. Micro-Level Traffic Simulation of Critical Road Sections

Several high-risk road sections (which featured considerable traffic flow and were easily affected by the simulated earthquake) were selected to evaluate the traffic conditions of roads under congested and blocked states to further study the traffic problems caused by the deterioration of road traversability following an earthquake.

(1) Congested State

The road sections with dense traffic flows were selected to conduct normal and congested state microsimulations; the results are shown in Figure 12.

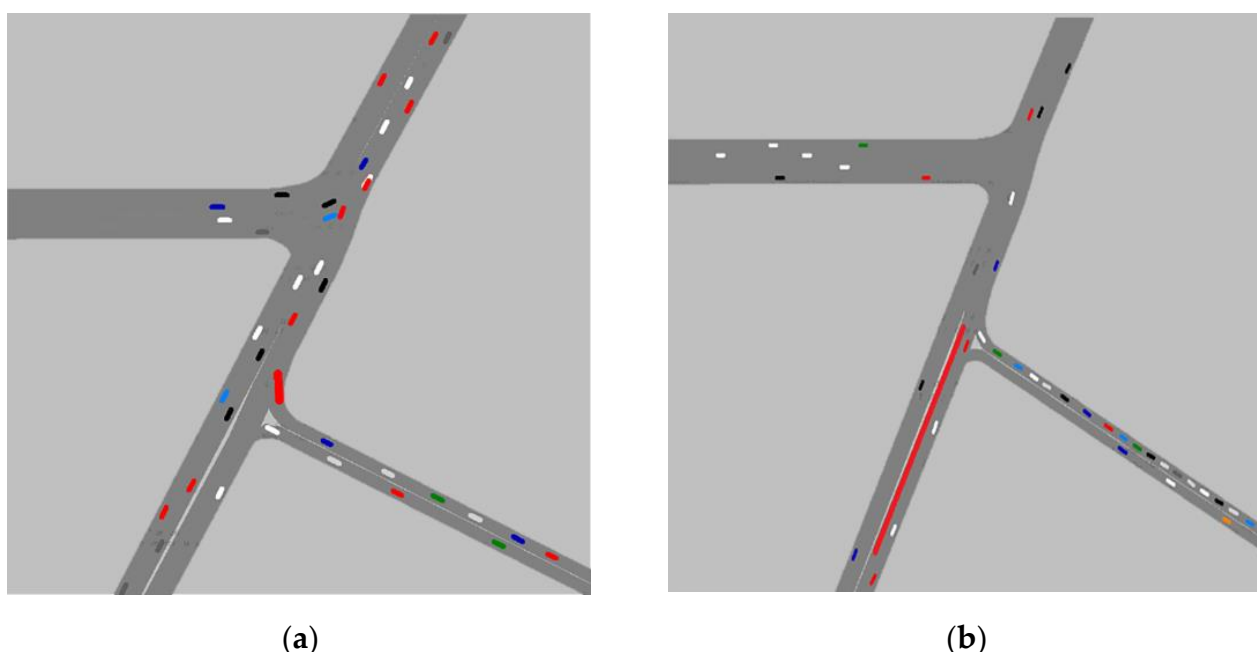


Figure 12. Comparison of simulation results under normal state and congested state at a certain time: (a) normal state; (b) congested state.

The red lines in Figure 12b indicate the specific parts of the lanes that were unavailable for vehicle passage. Compared to the results in Figure 12a, the upward running vehicles on this road section can only merge into the right lane, co-using the same lane as the upward running vehicles adjacent; thus, the vehicles about to merge into the right lane may have to queue. As a result, the road section shows a traffic jam, increasing traffic time.

To verify the above analysis, the average vehicle queuing times under the two scenarios were compared, as shown in Figure 13. Under normal conditions, as the simulation time increases, the average vehicle queuing time remains stable; in the congested state, the average vehicle queuing time increases linearly with simulation time owing to lane changes and other behaviors, exhibiting a maximum growth rate of 140% and proving that the traffic situation in high-risk sections can be considerably affected by changes in road traversability following an earthquake.

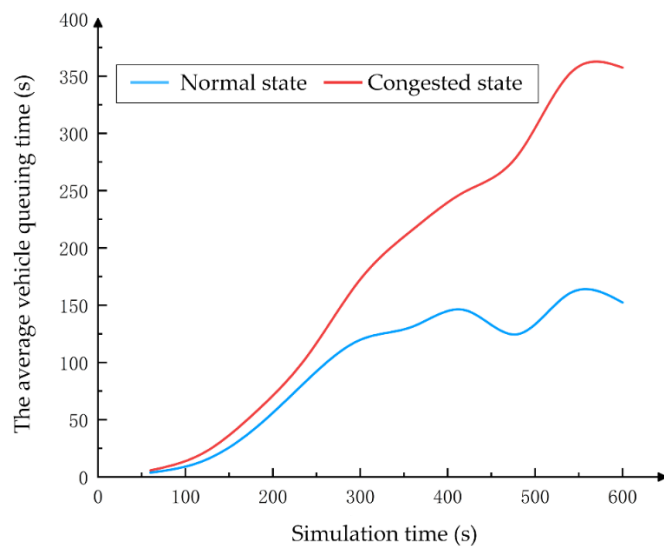


Figure 13. The average vehicle queuing times under the two scenarios.

(2) Blocked State

Local roads may be temporarily impassable following an earthquake, leading to a sharp increase in traffic flow on adjacent roads over a short period of time, which can readily cause road congestion. To simulate the road traffic in the blocked state, it was assumed that the end part of the selected road in the network was blocked. The microsimulation results are shown in Figure 14 in which the red line segment indicates the location of the completely blocked road.

In Figure 14, once the road on the upper right is completely blocked, the upward running vehicles can only turn left to merge into the right lane of the road on the left side; meanwhile, vehicles on the left road that want to turn left cannot continue to pass and can only merge into the downward running lane. Thus, the right lane of the road on the left side of the figure is likely to be congested by a large increase in traffic flow over a short period of time.

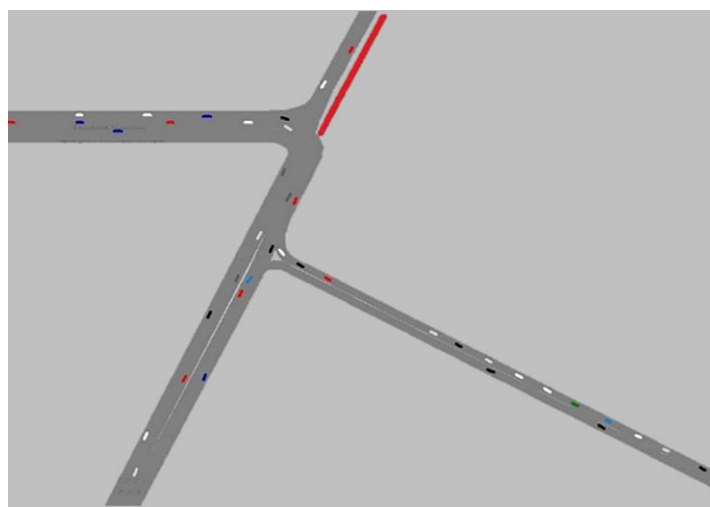


Figure 14. The simulation results under the blocked state.

To verify these analysis results, traffic data for the right lane of the road on the left side before and after the blockage are compared in Figure 15, indicating a significant increase in lane occupancy (approximately 100%) compared to normal conditions. In addition, the average speed of the vehicles in this lane decreases correspondingly, indicating that road

blockage would indeed have a considerable impact on the vehicle passing time following an earthquake.

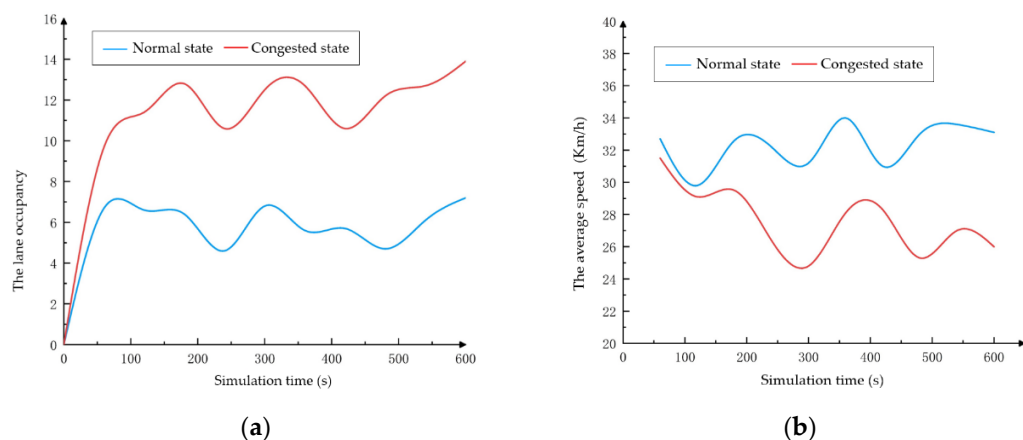


Figure 15. Comparison of simulation results under normal state and blocked state: (a) the change in lane occupancy; (b) the change in average speed.

5. Conclusions

In this study, the post-earthquake traffic conditions were simulated, considering the road traversability induced by building collapse and fires following an earthquake. Some conclusions can be drawn as follows:

- (1) A road traversability analysis solution considering the impact ranges of the earthquake-induced building collapse and post-earthquake fires was proposed by which the post-earthquake road traversability under multiple disasters can be analyzed.
- (2) A micro-level traffic simulation model considering road traversability following an earthquake was established to analyze the post-earthquake road traffic conditions and was validated against the measured data.

(3) The proposed post-earthquake traffic simulation method considering road traversability was applied to the Tongzhou district in Beijing. The simulation results show that the vehicle queuing time increased linearly by up to 140% owing to following and lane-changing behaviors caused by road blockage; these behaviors also significantly increased the occupancy of the surrounding lanes by approximately 100%. These results can help to determine specific traffic control measures and provide a reference for the decision-making of post-earthquake evacuation and rescue.

The simulation method proposed in this study can be used to evaluate the traversability of a regional road network suffering from building collapse debris and building fire spread following an earthquake and thereby simulate the traffic in key road sections. However, owing to the complex transportation system, the proposed method does not consider the impact of some factors, such as earthquake damage on bridges and post-earthquake road maintenance and clearing, which will be considered in a follow-up study. Additionally, because Beijing is used as a case in this study and there is a dearth of earthquake-related data in Beijing, the post-earthquake travel mode does not consider the change after the earthquake. More earthquake-prone regions will be studied in future research to consider this change.

Author Contributions: Conceptualization, Z.X.; methodology, Z.X. and Y.W.; investigation, Y.W. and C.L.; formal analysis, Z.X., Y.W. and C.L.; writing—original draft, Y.W.; writing—review and editing, Z.X. and R.S.; funding acquisition, Z.X. All authors have read and agreed to the published version of the manuscript.

Funding: This research was funded by General Program of the National Natural Science Foundation of China (Grant No. 51978049), Beijing Nova Program (Z191100001119115), Beijing Municipal Natural Science Foundation (Grant No. 8212011), Interdisciplinary Research Project for Young Teachers of

USTB (Fundamental Research Funds for the Central Universities) (Grant No. FRF-IDRY-20-030), and Scientific Research Fund of Institute of Engineering Mechanics, China Earthquake Administration (Grant No. 2019EEEVL0501).

Institutional Review Board Statement: Not applicable.

Informed Consent Statement: Not applicable.

Data Availability Statement: Not applicable.

Conflicts of Interest: The authors declare no conflict of interest.

References

1. Sasan, E.; Masoud, N.A. Performance of Transportation Systems in the 2003 Bam, Iran, Earthquake. *Earthq. Spectra* **2005**, *21*, 455–468. [[CrossRef](#)]
2. Moya, L.; Mas, E.; Yamazaki, F.; Liu, W.; Koshimura, S. Statistical Analysis of Earthquake Debris Extent from Wood-Frame Buildings and Its Use in Road Networks in Japan. *Earthq. Spectra* **2020**, *36*, 209–231. [[CrossRef](#)]
3. Chang, S.E. Transportation Performance, Disaster Vulnerability, and Long-Term Effects of Earthquakes. In Proceedings of the Second EuroConference on Global Change and Catastrophe Risk Management, Laxenburg, Austria, 6–9 July 2000.
4. Takashi, U. The Great Hanshin-Awaji Earthquake and the Problems with Emergency Medical Care. *Ren. Fail.* **1997**, *19*, 633–645. [[CrossRef](#)]
5. Wang, W.; Zhang, N.; Wang, L.; Wang, Z.; Ma, D. A Study of Influence Distance and Road Safety Avoidance Distance from Postearthquake Building Debris Accumulation. *Adv. Civ. Eng.* **2020**, *2020*, 7034517. [[CrossRef](#)]
6. Golla, A.P.S.; Bhattacharya, S.P.; Gupta, S. The Accessibility of Urban Neighborhoods When Buildings Collapse Due to an Earthquake. *Transp. Res. Part D Transp. Environ.* **2020**, *86*, 102439. [[CrossRef](#)]
7. Yu, Y.C.; Gardoni, P. Predicting Road Blockage Due to Building Damage Following Earthquakes. *Reliab. Eng. Syst. Saf.* **2022**, *219*, 102439. [[CrossRef](#)]
8. Argyroudis, S.; Selva, J.; Gehl, P.; Pitilakis, K. Systemic Seismic Risk Assessment of Road Networks Considering Interactions with the Built Environment. *Comput.-Aided Civ. Infrastruct. Eng.* **2015**, *30*, 524–540. [[CrossRef](#)]
9. Lo, I.T.; Lin, C.Y.; Yang, C.T.; Chuang, Y.J.; Lin, C.H. Assessing the Blockage Risk of Disaster-Relief Road for a Large-Scale Earthquake. *KSCE J. Civ. Eng.* **2020**, *24*, 3820–3834. [[CrossRef](#)]
10. Hirokawa, N.; Osaragi, T. Earthquake Disaster Simulation System: Integration of Models for Building Collapse, Road Blockage, and Fire Spread. *J. Disaster Res.* **2016**, *11*, 175–187. [[CrossRef](#)]
11. Kilanitis, I.; Sextos, A. Impact of Earthquake-Induced Bridge Damage and Time Evolving Traffic Demand on the Road Network Resilience. *J. Traffic Transp. Eng.* **2019**, *6*, 35–48. [[CrossRef](#)]
12. Hou, B.-W.; Li, X.-J.; Han, Q.; Liu, A.-W.; Lan, R.-Q. Post-Earthquake Connectivity and Travel Time Analysis of Highway Networks Based on Monte Carlo Simulation. *China J. Highw. Transp.* **2017**, *30*, 287–296. [[CrossRef](#)]
13. Chang, L.; Elnashai, A.S.; Spencer, B.F. Post-Earthquake Modelling of Transportation Networks. *Struct. Infrastruct. Eng.* **2012**, *8*, 893–911. [[CrossRef](#)]
14. Feng, K.; Li, Q.; Ellingwood, B.R. Post-Earthquake Modelling of Transportation Networks Using an Agent-Based Model. *Struct. Infrastruct. Eng.* **2020**, *16*, 1578–1592. [[CrossRef](#)]
15. Lu, X.; Guan, H. *Earthquake Disaster Simulation of Civil Infrastructures: From Tall Buildings to Urban Areas*; Springer: Singapore, 2017.
16. Lu, X.; Han, B.; Hori, M.; Xiong, C.; Xu, Z. A Coarse-Grained Parallel Approach for Seismic Damage Simulations of Urban Areas Based on Refined Models and Gpu/Cpu Cooperative Computing. *Adv. Eng. Softw.* **2014**, *70*, 90–103. [[CrossRef](#)]
17. Nishino, T.; Tanaka, T.; Hokugo, A. An Evaluation Method for the Urban Post-Earthquake Fire Risk Considering Multiple Scenarios of Fire Spread and Evacuation. *Fire Saf. J.* **2012**, *54*, 167–180. [[CrossRef](#)]
18. Chen, Y.; Eguchi, R.T. Post-Earthquake Road Unblocked Reliability Estimation Based on an Analysis of Randomicity of Traffic Demands and Road Capacities. In Proceedings of the 6th U.S. Conference and Workshop on Lifeline Earthquake Engineering (TCLEE) 2003, Long Beach, CA, USA, 10–13 August 2003; pp. 916–925.
19. Song, R.; Sun, J. Calibration of a Micro-Traffic Simulation Model with Respect to the Spatial-Temporal Evolution of Expressway on-Ramp Bottlenecks. *Simulation* **2016**, *92*, 535–546. [[CrossRef](#)]
20. Pell, A.; Meingast, A.; Schauer, O. Trends in Real-Time Traffic Simulation. *Transp. Res. Procedia* **2017**, *25*, 1477–1484. [[CrossRef](#)]
21. Lu, X.; Lu, X.; Guan, H.; Ye, L. Collapse Simulation of Reinforced Concrete High-Rise Building Induced by Extreme Earthquakes. *Earthq. Eng. Struct. Dyn.* **2013**, *42*, 705–723. [[CrossRef](#)]
22. Xiong, C.; Lu, X.; Lin, X.; Xu, Z.; Ye, L. Parameter Determination and Damage Assessment for Tha-Based Regional Seismic Damage Prediction of Multi-Story Buildings. *J. Earthq. Eng.* **2017**, *21*, 461–485. [[CrossRef](#)]
23. Lu, X.; Zeng, X.; Xu, Z.; Guan, H. Physics-Based Simulation and High-Fidelity Visualization of Fire Following Earthquake Considering Building Seismic Damage. *J. Earthq. Eng.* **2019**, *23*, 1173–1193. [[CrossRef](#)]
24. Xu, Z.; Zhang, Z.; Lu, X.; Zeng, X.; Guan, H. Post-earthquake fire simulation considering overall seismic damage of sprinkler systems based on BIM and FEMA P-58. *Autom. Constr.* **2018**, *90*, 9–22. [[CrossRef](#)]

25. Scawthorn, C.; O'Rourke, T.D.; Blackburn, F.T. The 1906 San Francisco earthquake and fire: Enduring lessons for fire protection and water supply. *Earthq. Spectra* **2006**, *22*, 135–158. [CrossRef]
26. Nishino, T.; Tsuburaya, S.I.; Himoto, K.; Tanaka, T. A study on the estimation of the evacuation behaviors of Tokyo city residents in the Kanto Earthquake Fire: Development of a potential-based evacuation model in post-earthquake fire. *Fire Saf. Sci.* **2008**, *74*, 105–114. [CrossRef]
27. Architect, S.A. Lessons from the Great Hanshin-Awaji Earthquake. Available online: <http://www3.grips.ac.jp/~ando/HanshinLessons%20en.pdf> (accessed on 8 August 2022).
28. Ren, A.; Xie, X. The Simulation of Post-Earthquake Fire-Prone Area Based on Gis. *J. Fire Sci.* **2004**, *22*, 421–439. [CrossRef]
29. Himoto, K.; Mukaibo, K.; Akimoto, Y.; Kuroda, R.; Hokugo, A.; Tanaka, T. A Physics-Based Model for Post-Earthquake Fire Spread Considering Damage to Building Components Caused by Seismic Motion and Heating by Fire. *Earthq. Spectra* **2013**, *29*, 793–816. [CrossRef]
30. Xie, X.; Ren, A. Dynamic Simulation of Fire Following Earthquake Based on Gis. *Strateg. Study CAE* **2007**, *2007*, 82–87. [CrossRef]
31. GB 50016-2014; Ministry of Housing and Urban-Rural Development of People's Republic of China. Code for Fire Protection Design of Buildings. China Planning Press: Beijing, China, 2014.
32. GB 50137-2011; Administration of Quality Supervision Inspection and Quarantine. Code for Classification of Urban Land Use and Planning Standards of Development Land. China Architecture & Building Press: Beijing, China, 2010.
33. Beijing Transportation Institute. List. Available online: <https://www.bjtrc.org.cn/> (accessed on 3 January 2020).
34. Beijing Transport Institute. *Beijing Transport Development Annual Report*; Beijing Transport Institute: Beijing, China, 2010.
35. Tao, S.; Ye, X. Forecasting Model of Intercity Trip Distribution with Consideration of Connections between Headquarters and Subsidiaries. *J. Tongji Univ.* **2020**, *48*, 1319–1327. [CrossRef]
36. Wang, X. Applicability Analysis of User Equilibrium Model (Ue) and Stochastic User Equilibrium Model (Sue) in Traffic Flow Assignment. *Sci. Technol. Innov.* **2019**, *2019*, 40–41. [CrossRef]
37. Cheng, X.; Liu, Y.; Guo, J. Method of Quantifying Uncertainty Inuser Equilibrium Traffic Assignment. *J. Nanjing Univ. Inf. Sci. Technol.* **2019**, *11*, 421–427. [CrossRef]
38. PTV Group. Ptv-Vissim. Available online: <https://www.ptvgroup.com/en/solutions/products/ptv-vissim/> (accessed on 22 April 2020).
39. Fu, C.; Gao, M.; Yu, Y. Studying on Amplification Effect of Beijing Basin on 3~10 S Ground Motion by Numerical Simulation Method. *J. Seismol. Res.* **2015**, *38*, 448–460. [CrossRef]